ELECTRON BEAM PROFILE MEASUREMENTS WITH VISIBLE AND X-RAY SYNCHROTRON RADIATION AT THE SWISS LIGHT SOURCE

Åke Andersson, Volker Schlott, Martin Rohrer, Andreas Streun, PSI, Villigen, Switzerland
Oleg Chubar, SOLEIL, Gif-sur-Yvette, France

Abstract

Two different methods of beam profile measurement using a) visible-to-UV range synchrotron radiation and b) X-ray synchrotron radiation have been realized in a single diagnostics beam line at the Swiss Light Source (SLS). While the visible-to-UV part uses a focusing lens to create an image of the electron beam cross section, the X-ray part makes use of the pinhole camera principle. In the visible-to-UV case the vertically polarized synchrotron radiation renders an image heavily influenced by inherent emission and diffraction effects of synchrotron radiation. This turns out to be an advantageous influence in order to determine ultra small beam profiles. For the visible-to-UV branch practical point-spread function measurements, including all beam line components and high-precision wave-optics based calculations of the synchrotron light characteristics were performed (SRW-code [1]) to ensure correct interpretation of the measured profiles. Also the X-ray branch was simulated by SRW. Results from both monitors will be presented to allow for comparison.

INTRODUCTION

Emittance measurements of synchrotron radiation (SR) sources are facing higher and higher demands while the development goes towards higher brilliance. Usually the SR is used to form an image of the beam cross-section, and when knowing the beam size at the observation point the emittance is derived from the machine functions. The high brilliance gives two main problems. One is that the higher the current, the higher the thermal load on the first optical element. The other is the fact that inherent features of SR emission and diffraction effects contribute increasingly to the measured beam profile with decreasing emittance. At SLS we have chosen the image formation method, but in two widely separated regions of the SR spectrum, the visible and the hard X-ray. Both methods have been used at several SR labs, but in the visible we additionally make use of the vertically polarised light, a technique developed at MAX-lab [2].

THE DIAGNOSTIC BEAMLINE

The source point of the beamline is the centre of the middle bending magnet in the SLS' triple bend achromat lattice (see Table 1 for machine parameters). The X-ray branch uses only 0.8 mrad$_H$, while the visible branch immediately next to it, has a clearance of 7 mrad$_H$ x 7 mrad$_V$. Roughly 4m from the source point (sp) the water cooled pinhole array made of a 150μm thick Tungsten sheet, with 104 15μm diameter holes sits. The light escaping these holes carries negligible power and is let out in air through a 250μm thick Aluminium window.

In the visible branch the light is angled 90 degrees twice to direct the light parallel, with 0.35m separation, to the X-rays. The first mirror is made of SiC, a material which has a very advantageous ratio of thermal conductivity and expansion. This helps for low current measurements at moderate heat load (a few tens of Watts). However, for higher currents we have implemented a "thin absorber" which can be inserted before the mirror, obstructing only the mid ±0.45 mrad$_V$ of the SR. This takes away almost all of the 400 Watt heat load on the mirror at full current. The second mirror is a movable aluminized fused silica (FS) mirror. In between a FS spherical lens (5m from sp) is situated. These three optical components are chosen with λ/20 surface accuracy. The visible-to-UV light is brought out of vacuum only at the end of the beamline (9m from sp), through a FS vacuum window. Molybdenum filters and phosphor (P43) for the X-ray branch, grey filters, bandpass (BP) filters, a polarizer for the visible branch and the two CCD cameras are placed on an optical table at the end of the beamline, which is still inside the ring tunnel. The visible branch camera can be remotely moved longitudinally when different BP filters are used, since the lens' focal length is wavelength dependant; the X-ray branch camera has a zoom and focus adjustable lens system. For the visible, an online point-spread-function measurement setup is under development.

Table 1: Some SLS parameters

Energy	2.4 GeV
Dipole field	1.4 T
Nom. Hor. Emittance	5.5 nmrad
Nat. Energy Spread	0.086%
βx ; βy ; ηx (at obs.point)	0.45m;14.3m;29mm

THEORETICAL FRAMEWORK

A wave-optics based treatment of SR diffraction and focusing are given in [3] and [4]. While [3] is a pioneer work giving the qualitative results, [4] gives the foundation for quantitative calculations, and supplies the basis for the SRW-code. In the visible-to-UV case diffraction effects and inherent features of the SR emission have been simulated by the SRW-code giving "filament-beam"-spread-functions (FBSF), the equivalent to point-spread-functions in the case of virtual point sources. Convoluting the FBSF with a Gaussian distribution (or any assumed electron distribution) should give the measured image profile. In the case of focused vertically polarised light from a bending magnet the FBSF, in the vertical direction, is a two-peaked distribution with a zero minima in the centre (for 2-dim. visualisation please see [5]). For an increasing vertical

beam size this minimum becomes more shallow. The valley-to-peak ratio is only marginally affected in the case of the thin absorber obstructing the mid part of SR, even though the tail intensities are increased. Also the X-ray case was simulated wih SRW. The result is a FBSF with a slightly smaller width than estimated by adding in square contributions from Fraunhofer diffraction and geometrical blurring due to the finite pinhole size.

MEASUREMENTS

To draw the comparison between the two branches of the beamline, we chose two modes of operation, both at 10 mA of circulating current. One mode was the usual user operation mode (except for the low current) and the other mode was with reduced sextupole strengths.
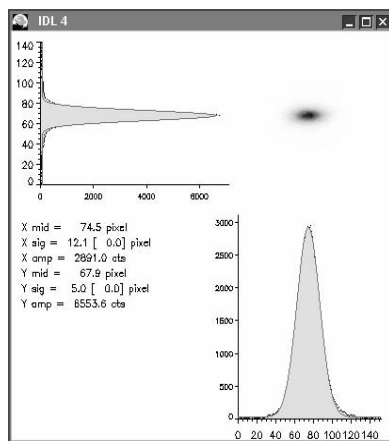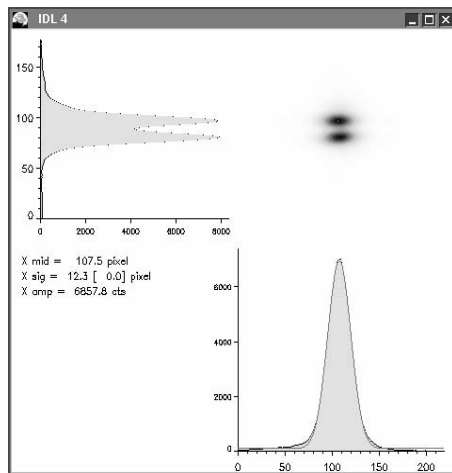
We compare the two types of measurement methods, the Visible Vert. Polarized and the X-ray pinhole camera method. Figures 1 and 2 show the measured image profiles. Where applicable, a Gaussian fit is shown with its σ –value in units of pixels. Figure captions give pixel size, imaging ratio and also $\sigma_{x,yimage}$ in μm after converting to a 1:1 imaging. The Gaussian fit and its corresponding σ –value is only an approximation, but makes comparison easier. In the Visible Vertically Polarised method, only the ratio valley-to-peak intensity is needed to derive the vertical beam size.
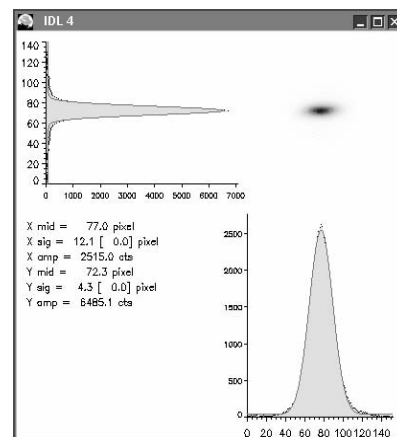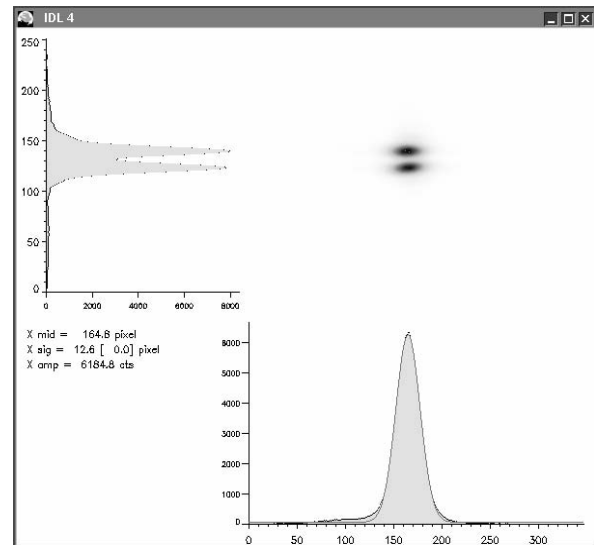

Figure 1: Image taken at 10 mA in user op. mode. Top: Vert. polarised image at 365nm. Pixel size 4.65μm, image ratio 1:0.838. At 1:1 imaging, σ_{ximage} = 68 μm , I_v/I_p = 0.54. Bottom: X-ray pinhole camera image. Pixel size 6.0μm, image ratio 1:1.27. At 1:1 imaging, σ_{ximage} = 57 μm , σ_{yimage} = 24 μm.

Figure 2: Image taken at 10 mA with reduced sextupole strengths. Top: Vert. polarised image at 365nm. Pixel size 4.65μm, image ratio 1:0.838. At 1:1 imaging, σ_{ximage} = 70 μm , I_v/I_p = 0.39. Bottom: X-ray pinhole camera image. Pixel size 6.0μm, image ratio 1:1.27. At 1:1 imaging, σ_{ximage} = 57 μm , σ_{yimage} = 20 μm.

06 Beam Instrumentation and Feedback
T03 Beam Diagnostics and Instrumentation

In Table 2 we have summarized the measured image sizes (σ_{ximage} and σ_{yimage}) converted to 1:1 imaging, the valley to peak intensity for the vertically polarised case, and the derived beamsizes (σ_x and σ_y).

Table 2: Measurement summary at 10mA.

10 mA	Ver pol 365nm		X-ray	
	σ_{ximage}	σ_x	σ_{ximage}	σ_x
User mode	68μm	61μm	57μm	56μm
	I_v/I_p	σ_y	σ_{yimage}	σ_y
User mode	0.54	19μm	24μm	20μm
Red. Sext.mode	0.39	15μm	20μm	16μm

Fig. 3 shows a measured beam profile at 300 mA with the thin absorber obstructing the central part of the SR. Note the slightly increased portion of light in the tails. The derived vertical beam size is in this case $\sigma_y = 17$μm, corresponding to a vertical emittance of $\varepsilon_y = 19$pmrad (coupling 0.35%).
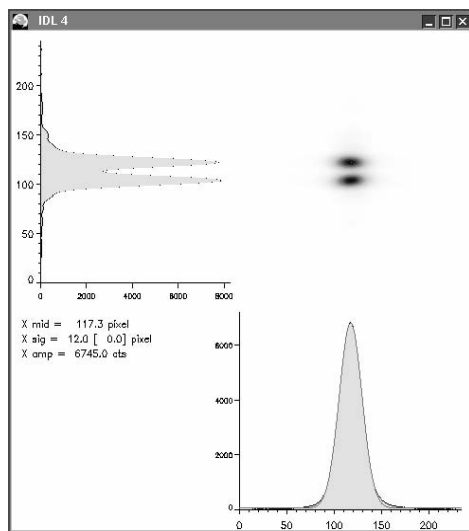

Figure 3: Image taken at 300 mA user op. mode. Observation wavelength 400nm, with the thin absorber obstructing the middle part of SR. I_v/I_p = 0.40 corresponding to $\sigma_y = 17$μm.

Table 3: Measurement summary at 300 mA.

300 mA	Ver pol 400nm		X-ray	
User mode, f-wigg. 12.8mm	σ_{ximage}	σ_x	σ_{ximage}	σ_x
	71μm	63μm	62μm	61μm
User mode, f-wigg. 12.8mm	I_v/I_p	σ_y	σ_{yimage}	σ_y
	0.40	17μm	24μm	20μm

Measurements were also performed at 300 mA user operation. In this case the FEMTO-wiggler [6] was partly closed, giving an increased horizontal emittance. The nominal emittance and a natural energy spread would give $\sigma_x = 56$μm. Table 3 summarizes these results.

DISCUSSION AND OUTLOOK

In view of accuracy, it is desirable for the X-ray branch if the "filament-beam"-spread-function (FBSF) is significantly smaller than the measured image size. If not, one is in simple words making a quadratic subtraction of two similar numbers which could lead to uncertainty. For the visible branch the vertically polarized image is highly dominated by the FBSF. However, the valley-to peak ratio in the image is still very sensitive to the vertical beam size, which allows for good accuracy. If a small vertical beam size is reached (by better coupling control), this ratio will go towards zero. The remedy will be to observe at a shorter wavelength, where again the valley becomes more shallow. For the moment observation at 400 nm matches the SLS operating conditions, but the visible-to-UV branch is prepared to measure down to 250 nm if necessary. We are also investigating the possibilities to further minimize the FBSF for the X-ray branch. Even though relative changes of approx. 1μm are detected in both branches, further work is foreseen to investigate the absolute differences between methods in the few μm range.

REFERENCES

[1] O. Chubar, P. Ellaume, Proc. of EPAC'98, 6th EPAC, 1998, p.1177.

[2] Å. Andersson, Ph.D. thesis work, ISBN 91-628-2686-7, and Å. Andersson, M. Eriksson, O. Chubar, Proc. of EPAC'96, 5th EPAC,1996, p 1689.

[3] A. Hofmann, F. Meot, Nucl. Instr. And Meth. 203 (1982), p. 483.

[4] O. Chubar, Proc. of IEEE PAC'93, Vol. 3, 1993, p. 2510.

[5] O. Chubar, P. Ellaume, A. Snigerev, Nucl. Instr. And Meth. A 435 (1999), p. 495.

[6] A. Streun et. al, "Sub-picosecond X-ray Source FEMTO at SLS", these proceedings.